

# Sparse Bayesian Modeling of EEG Channel Interactions Improves P300 Brain-Computer Interface Performance

Guoxuan Ma\*, Yuan Zhong\*, Moyan Li\*, Yuxiao Nie, and Jian Kang<sup>†</sup>  
Department of Biostatistics, University of Michigan, Ann Arbor MI 48109

March 2, 2026

## Abstract

Electroencephalography (EEG)-based P300 brain-computer interfaces (BCIs) enable communication without physical movement by detecting stimulus-evoked neural responses. Accurate and efficient decoding remains challenging due to high dimensionality, temporal dependence, and complex interactions across EEG channels. Most existing approaches treat channels independently or rely on black-box machine learning models, limiting interpretability and personalization. We propose a sparse Bayesian time-varying regression framework that explicitly models pairwise EEG channel interactions while performing automatic temporal feature selection. The model employs a relaxed-thresholded Gaussian process prior to induce structured sparsity in both channel-specific and interaction effects, enabling interpretable identification of task-relevant channels and channel pairs. Applied to a publicly available P300 speller dataset of 55 participants, the proposed method achieves a median character-level accuracy of 100% using all stimulus sequences and attains the highest overall decoding performance among competing statistical and deep learning approaches. Incorporating channel interactions yields subgroup-specific gains of up to 7% in character-level accuracy, particularly among participants who abstained from alcohol (up to 18% improvement). Importantly, the proposed method improves median BCI-Utility by approximately 10% at its optimal operating point, achieving peak throughput after only seven stimulus sequences. These results demonstrate that explicitly modeling structured EEG channel interactions within a principled Bayesian framework enhances predictive accuracy, improves user-centric throughput, and supports personalization in P300 BCI systems.

*Keywords:* Brain-Computer Interface, Bayesian Method, Gaussian Process, P300 Speller

---

\*Equally contributed

<sup>†</sup>To whom correspondence should be addressed: [jjankang@umich.edu](mailto:jjankang@umich.edu)

# 1 Introduction

Brain-computer interfaces (BCIs) facilitate direct communication between the human brain and external devices such as computers. The widespread interest in BCI systems stems from their broad range of potential applications in movement and communication assistance, particularly for individuals with motor impairments (Pfurtscheller et al. 2008), while their applications include performance enhancement in healthy users, neurorehabilitation, and other cognitive and clinical research domains (Van Erp et al. 2012, Kwak et al. 2015).

The BCI systems typically acquire brain activity through noninvasive electroencephalography (EEG). Among various EEG signals, event-related potentials (ERPs) refer to brain responses elicited by external stimuli such as visual, auditory, or somatosensory cues (Farwell & Donchin 1988). In an ERP-based BCI design, the system presents multiple stimuli in an on-screen keyboard, and the user focuses attention and mentally response to the desired stimulus. The stimulus that the user intends to select is called the target stimulus. After each stimulus presentation, the BCI classifies the corresponding EEG response as either target or non-target, depending on whether it contains ERP components of target perception. This design is often named after the P300 component, a deflection in the EEG signal that peaks approximately 300 ms after the onset of a rare or unexpected target stimulus (Fazel-Rezai et al. 2012). Among various applications of P300-based BCIs, the P300 speller is one of the most well-known. It functions as a virtual keyboard which allows users to type characters by attending to flashing groups of letters or symbols, which are then decoded based on the elicited P300 responses (Farwell & Donchin 1988).

**Data and motivation** To better illustrate the problem, we briefly describe the motivating EEG dataset from a publicly available P300-based BCI experiment by Won et al. (2022). The study collected EEG recordings from 55 participants during BCI spelling tasks, together with questionnaire data on demographics and physical and mental states

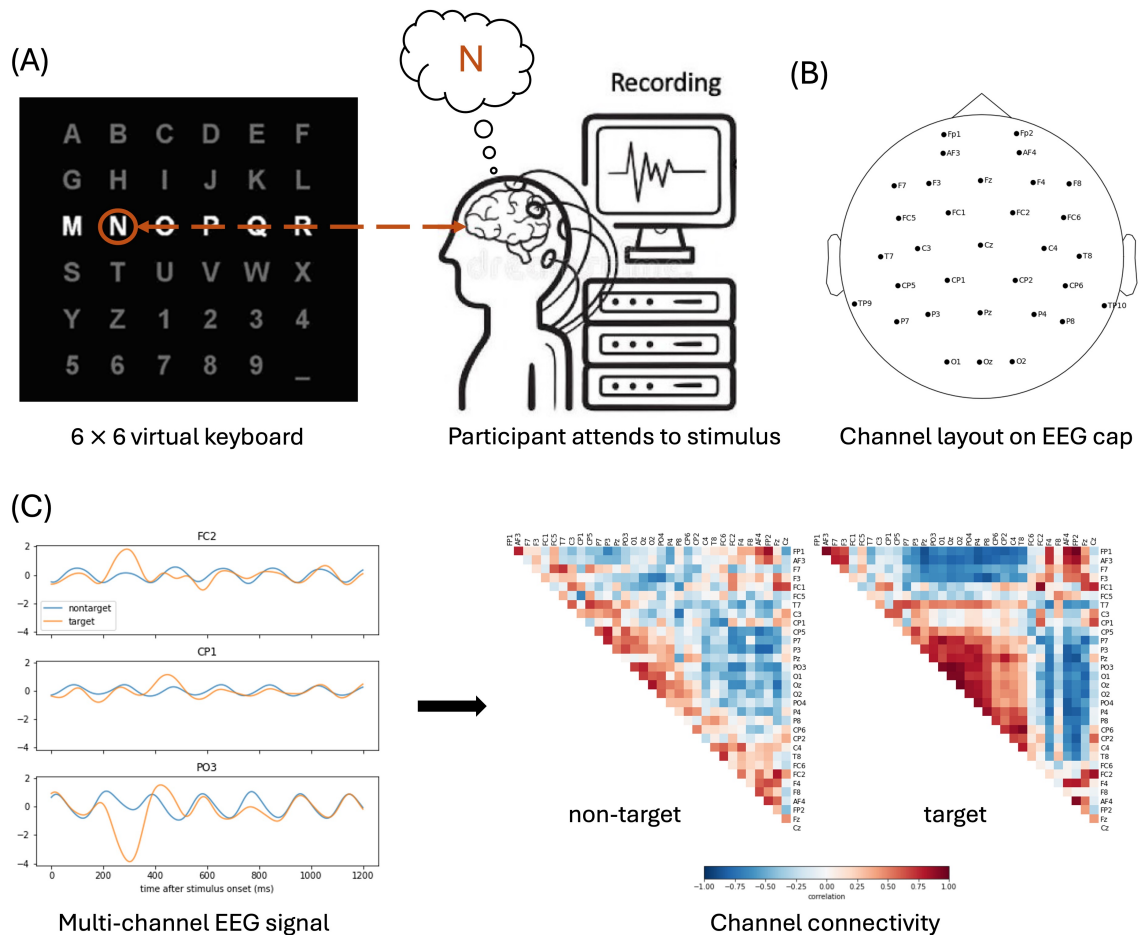


Figure 1: An illustration of the P300 BCI spelling task and recorded signal. (A) The P300 BCI speller presents a sequence of row or column flashes (a row or a column) on a virtual screen to the user. The user focuses on a target character and responds to the row and column flashes that contain the target character. The EEG signals of the flash are recorded from multiple channels and are segmented into a 1200 ms window following stimulus onset. (B) The names and layout of the 32 scalp EEG channels according to the international 10-20 system. (C) Example of recorded multi-channel EEG signals and the derived channel connectivity.

before and after the experiment. Each participant completed both a calibration (training) phase and a test phase using a P300 speller. During spelling, rows and columns of a virtual keyboard (a  $6 \times 6$  matrix; see Figure 1A) were flashed repeatedly in a random order. As a result, each stimulus sequence was consisted of 12 flashes (i.e., 6 rows and 6 columns). For a given target character, the flashes corresponding to its row and column constituted target stimuli, while all remaining flashes were non-targets. Each character selection included 15 such stimulus sequences. EEG signals were recorded from 32 scalp

channels arranged according to the international 10-20 system and segmented into 1200 ms windows following the stimulus onset to capture the event-related responses associated with the P300 component. More details are available in Section 4.

As illustrated in Figure 1C, discriminative information between target and non-target signals varies across channels and time. For example, channels FC2 and PO3 show clear target-related deflections in the P300 latency range, whereas channel CP1 exhibits much weaker differences. Even within informative channels, only limited post-stimulus time intervals contribute meaningfully to discrimination. These motivates temporal channel selection via sparse modeling to reduce noise from uninformative channels and time points. Beyond marginal temporal features, the signal interactions between EEG channels, summarized through measures of channel connectivity, provide an additional and complementary source of discriminative information. Figure 1C shows that the connectivity patterns derived from the target signal differ from those of non-target signals. Incorporating channel connectivity as an additional predictor, alongside temporal EEG features, therefore has the potential to improve classification performance. Furthermore, because subject-level questionnaire data on demographics and physical and mental states are available, this dataset enables investigation of heterogeneity across individuals, including whether certain subgroups of participants benefit more from accounting for signal interactions in modeling than others. This opens the door to identifying populations for whom modeling channel interactions is particularly advantageous, with implications for personalized and adaptive BCI systems.

**Related work** The most-studied and fundamental computational challenge in P300-based BCIs is the classification of brain activity following each stimulus as either a target or non-target response. Accurate classification of these EEG segments enables the identification of the target row and column in the speller matrix, and hence the selection of the desired character. The original work (Farwell & Donchin 1988) developed four classification

methods, stepwise linear discriminant analysis (SWLDA), peak picking, area, and covariance, with the best performance achieved by SWLDA in their experiment. Subsequent studies have sought to improve P300 speller performance through more advanced machine learning and signal processing techniques, including independent component analysis (ICA) (Xu et al. 2004) and support vector machines (SVMs) (Kaper et al. 2004). A comprehensive review by Philip & George (2020) highlighted the strength of ensemble methods, which combine the advantages of multiple classifiers and are particularly effective for handling the class imbalance inherent in P300 datasets. Bayesian methods have also gained increasing attention for BCI classification. For example, Zhang et al. (2015) proposed a sparse Bayesian model using Laplace priors for EEG signal classification. Barthélemy et al. (2023) introduced a Bayesian accumulation of Riemannian probabilities, providing an end-to-end framework for P300 BCI classification. Recently, Ma et al. (2022) developed a Bayesian generative model that characterizes the probability distribution of multi-trial EEG signals, which provides both a flexible simulation tool for EEG data and a novel probabilistic classifier for P300 BCIs.

Despite the success of existing methods, most approaches overlook potential functional relationships among brain regions and treat EEG signals from different channels as independent predictors. However, studies have shown that brain functions arise from the coordinated activity of distributed areas rather than isolated regions (Tononi & Edelman 1998, Friston et al. 1997). In the BCI context, Kabbara et al. (2016) demonstrated clear differences in functional brain networks between target and non-target visual stimuli. These findings suggest that interactions among EEG channels, which reflect network-level brain dynamics, carry important information for distinguishing stimulus types (target/non-target). Modeling such inter-channel dependencies can therefore enhance both the predictive accuracy and the neurophysiological interpretability of BCI systems.

To model signal interactions, many existing approaches adopt a two-step strategy, by

first identifying main effects and then refitting the model with both main and interaction effects (Hao et al. 2018, Wang et al. 2021). However, this approach is less suitable for EEG data, as the presence of an interaction does not necessarily depend on the existence of corresponding main effects. Zhao et al. (2025) took a difference approach by introducing the Gaussian Latent channel model with Sparse time-varying effects (GLASS) for P300 speller, which uses constrained multinomial logistic regression for target classification while accounting for correlations between channels via latent channel decompositions. Although GLASS incorporates channel correlations into the model structure, it does not explicitly model channel interactions as predictors, and therefore cannot directly evaluate and interpret the effect sizes of inter-channel relationships. Recent Bayesian approaches have incorporated both main and interaction terms within a unified inference framework using hierarchical shrinkage priors (Griffin & Brown 2017). Nonetheless, such general frameworks is less effective in accounting for the unique temporal and structural dependencies in EEG data. More recently, neural network-based methods have been proposed in EEG classification tasks. Examples include multi-task autoencoder models (Ditthapron et al. 2019), compact convolutional neural networks such as EEGNet (Lawhern et al. 2018), and weighted ensemble strategies (Kshirsagar & Londhe 2019). These approaches can implicitly capture interaction effects among EEG channels and their association with stimulus type outcomes. However, they often require extensive task-specific architectural design and large training datasets, which vary considerably across studies. Moreover, the black-box nature of neural networks limits interpretability, making it difficult to identify which specific channels or channel pairs drive classification decisions. This lack of interpretability constrains the scientific insights that can be drawn about the underlying neural mechanisms and may hinder model generalizability. Consequently, there is a strong need for statistical methods that can incorporate inter-channel interaction effects while preserving interpretability and computational efficiency.

**Our contributions** In this paper, we propose a Bayesian time-varying regression model with signal interactions via relaxed-thresholded Gaussian process (SI-RTGP) priors. Our model relaxes the traditional linearity assumption among EEG predictors by explicitly modeling signal interaction effects across channels, while performing temporal-spatial channel selection, thereby improving both predictive performance and interpretability. To our knowledge, this is among the first models to explicitly incorporate inter-channel interactions into EEG-based prediction within a Bayesian framework.

We propose a relaxed-thresholded Gaussian process (RTGP) prior to flexibly model the association between EEG signals and stimulus-type outcomes. It has several advantages compared to existing work. First, the RTGP prior defines a broad class of temporally varying functions that are piecewise smooth and sparse, which enables automatic feature selection with Bayesian inference. Second, compared with existing thresholded Gaussian process priors, such as the soft-thresholded (Kang et al. 2018) and hard-thresholded (Cai et al. 2020) variants, the proposed RTGP prior is more flexible, capable of adapting to both sparse and non-sparse patterns by tuning a relaxation parameter. It also offers substantial computational advantages, allowing efficient MCMC sampling even for large-scale EEG datasets. We evaluate the proposed method using both synthetic data and EEG data from the P300 speller study by Won et al. (2022). The SI-RTGP model achieves higher classification accuracy for many participants and identifies meaningful channels and channel pairs, which provides valuable insights into the neural mechanisms underlying P300 responses.

## 2 Method

### 2.1 Bayesian time-varying model with signal interactions

Our model is individual-specific, meaning that a separate model is built for each participant using only their own calibration data and evaluated on their corresponding test data. For clarity, the subject index is suppressed in the notation throughout the model development.

Suppose a total of  $R$  target characters are typed during the calibration phase. For each character  $r = 1, \dots, R$ , the BCI presents  $S$  stimulus sequences, each consisting of  $J = 12$  flashes: 6 row stimuli ( $j = 1, \dots, 6$ ) and 6 column stimuli ( $j = 7, \dots, 12$ ) on a  $6 \times 6$  speller matrix, in a random order. Let  $I = \{(r, s, j) \mid r = 1, \dots, R; s = 1, \dots, S; j = 1, \dots, J\}$  denote the index set of all stimulus presentations. The total number of flashes is therefore  $n = |I| = R \times S \times J$  flashes in total, and we use  $i \in I$  to index an individual flash. Let  $K$  denote the number of EEG channels and  $T$  the number of time points within the post-stimulus window. Then, denote  $X_{ki}(t)$  the observed intensity of the EEG signal of the  $i$ -th stimulus from channel  $k$  at time  $t$ . Let  $\mathbf{X}_{ki} = (X_{ki}(1), \dots, X_{ki}(T))^\top \in \mathbb{R}^T$  and  $\mathbf{X}_i = (\mathbf{X}_{1i}^\top, \mathbf{X}_{2i}^\top, \dots, \mathbf{X}_{Ki}^\top)^\top \in \mathbb{R}^p$ , where  $p = KT$ . We denote by  $Z_i(k_1, k_2)$  the signal interaction between channels  $k_1$  and  $k_2$ , where  $1 \leq k_1 < k_2 \leq K$ . In this study, we define the signal interaction as the Fisher Z-transformation of the Pearson correlation between  $\mathbf{X}_{k_1i}$  and  $\mathbf{X}_{k_2i}$ , i.e.

$$Z_i(k_1, k_2) = \frac{1}{2} \log \left\{ \frac{1 + \text{cor}(\mathbf{X}_{k_1i}, \mathbf{X}_{k_2i})}{1 - \text{cor}(\mathbf{X}_{k_1i}, \mathbf{X}_{k_2i})} \right\}.$$

Let  $\mathbf{Z}_i = \{Z_i(k_1, k_2)\}_{1 \leq k_1 < k_2 \leq K} \in \mathbb{R}^q$ , where  $q = K(K - 1)/2$ . Finally, let  $Y_i \in \{0, 1\}$  be the target/non-target stimulus type outcomes of the  $i$ -th flash. Figure 2 provides an illustration on data and notations.

We propose a Bayesian time-varying classification model with signal interactions to

Index mapping  $I = \{(r, s, j) \mid r = 1, \dots, R; s = 1, \dots, S; j = 1, \dots, J\}$   $i \in I$  index the stimulus

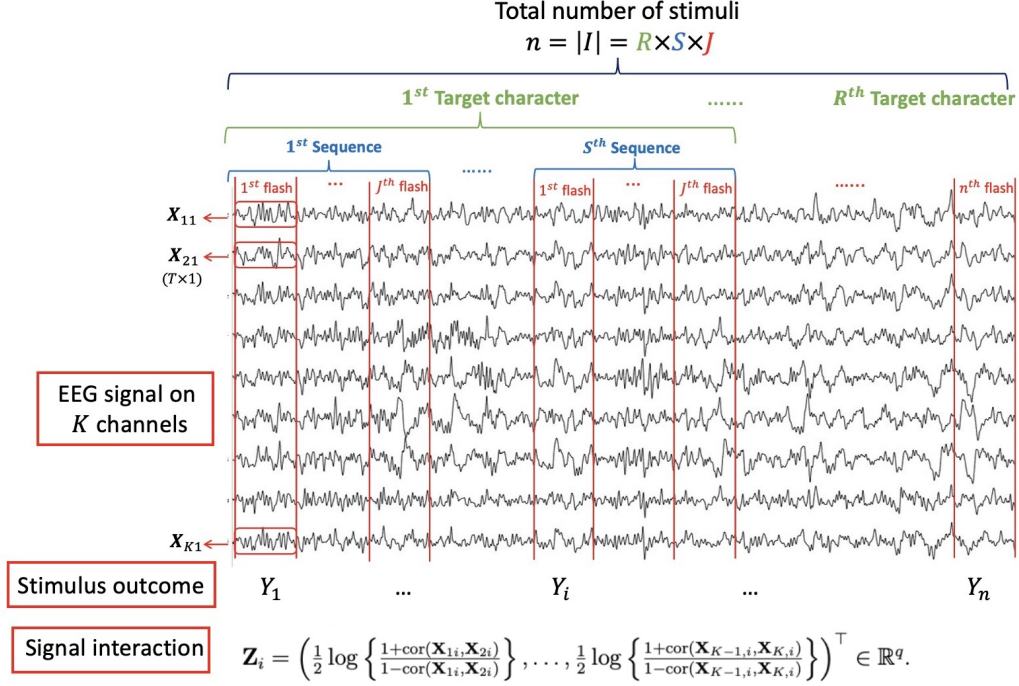


Figure 2: Illustration of the data and notation for the SI-RTGP model.  $\mathbf{X}_{ki}$  represents the EEG signal from channel  $k$  for the  $i$ -th flash. For the  $i$ -th flash, the signal interaction between channel  $k_1$  and channel  $k_2$  is measured by the z-transformed Pearson correlation between EEG signals from channels  $k_1$  and  $k_2$ .

predict the stimulus type outcome, as follows,

$$g \{ \Pr(Y_i = 1 \mid \mathbf{X}_i, \mathbf{Z}_i) \} = \frac{1}{p} \sum_{k=1}^K \sum_{t=1}^T \beta_k(t) X_{ki}(t) + \frac{1}{q} \sum_{k_1 < k_2} \zeta(k_1, k_2) Z_i(k_1, k_2), \quad (1)$$

where  $g(\cdot)$  is the link function (e.g., probit and logit),  $\beta_k(t)$  is a time-varying coefficient function for channel  $k$ , and  $\zeta(k_1, k_2)$  quantifies the effect of the signal interaction between the EEG signal from channels  $k_1$  and  $k_2$ . The rescaling factors  $1/p$  and  $1/q$  are introduced to prevent the linear predictor  $\mu_i$  from becoming excessively large when  $K$  and  $T$  are large. Model (1) accounts for signals from each separate channel and signal interactions across channels as predictors for stimulus type outcomes classification.

## 2.2 Relaxed-thresholded Gaussian process prior

Thresholded Gaussian process priors are effective in capturing both the sparsity and temporal dependency in the relationship between stimulus type and EEG signal predictors. However, existing variants, such as the soft-thresholded Gaussian process (Kang et al. 2018, Xu & Kang 2025, Xu et al. 2026) and the thresholded Gaussian process (Shi & Kang 2015, Wu et al. 2024), can pose significant computational challenges when applied to large-scale datasets. To address this, we propose a relaxed-thresholded Gaussian process (RTGP) prior, which maintains the ability to capture sparsity while improving computational efficiency, defined as follows.

**Definition 1.** *Given a kernel  $\kappa$ , a thresholding parameter  $\omega \geq 0$ , and a relaxing parameter  $\xi > 0$ , suppose  $f(x) \sim GP(0, \kappa)$  and  $\tilde{f}(x) \sim N(f(x), \xi^2)$ . Let  $g(x) = f(x)I(|\tilde{f}(x)| > \omega) \triangleq T_r(f, \omega, \xi^2)$ , then  $g(x)$  follows a relaxed-thresholded Gaussian process, denoted as  $g(x) \sim RTGP(\kappa, \omega, \xi^2)$ .*

In Definition 1,  $I(\cdot)$  denotes the indicator function and  $T_r$  is the relaxed-thresholding function. The introduction of  $\tilde{f}(x)$  allows the full conditional distribution of  $f(x)$  to have a conjugate and closed-form expression. The parameter  $\xi^2$  represents the variance of  $\tilde{f}(x)$  and serves as a relaxing parameter that controls the independent white noise added to  $f(x)$ . Smaller values of  $\xi^2$  impose a stricter constraint that preserves the mean structure of  $f(x)$ , while larger values provide greater flexibility. To illustrate, Figure 3 compares different thresholded GP functions. Let  $f(x) \sim GP(0, \kappa)$ . The soft-thresholding function  $T_s(f(x), 0.5)$  sets values with  $|f(x)| < 0.5$  to zero, and otherwise shrinks the magnitude by the threshold 0.5. The hard-thresholding function  $T_h(f(x), 0.5)$  also sets values below magnitude of 0.5 to zero, while leaving larger values unchanged. Both soft and hard thresholded GPs impose sparsity and piecewise smoothness, with the hard-thresholded GP introducing jump discontinuities and the soft-thresholded GP remaining continuous.

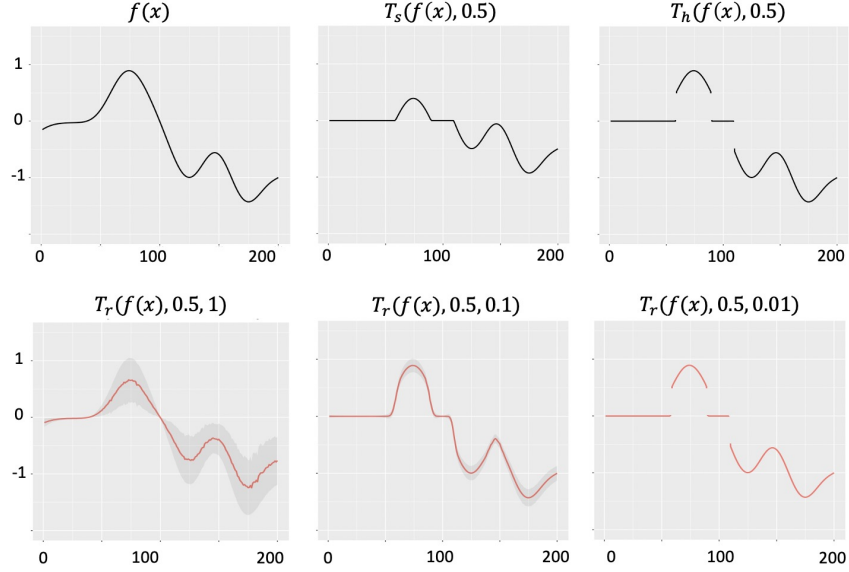


Figure 3: Illustration of different thresholded Gaussian process prior.  $T_s(\cdot, 0.5)$  and  $T_h(\cdot, 0.5)$  represents the soft and the hard thresholding function thresholded at 0.5.  $T_r(\cdot, 0.5, \xi^2)$  represents the proposed relaxed-thresholding function with different value of relaxing parameter  $\xi^2$ .

The second row of Figure 3 illustrates the proposed RTGP under different values of  $\xi$ . When  $\xi = 0.01$ ,  $T_r\{f(x), 0.5, 0.01\}$  closely resembles the hard-thresholded GP. For  $\xi = 0.1$ ,  $T_r\{f(x), 0.5, 0.1\}$  is a continuous function that preserves sparsity, similar to the soft-thresholded GP. As  $\xi$  increases to 1,  $T_r\{f(x), 0.5, 1\}$  recovers  $f(x)$ .

This flexibility is particularly valuable in modeling EEG data, where the true signal pattern is unknown. For example, if the true curve near  $x = 100$  is with meaningful magnitude as in 3, RTGP can adapt and recover the pattern by choosing an appropriate  $\xi$  (e.g.  $\xi = 1$ ), whereas both soft- and hard-thresholded GPs would enforce sparsity with probability 1. The following proposition formalizes the relationship between the RTGP and other thresholded GPs.

**Proposition 1.** *Given a thresholding parameter  $\omega > 0$ , let  $T_r(\theta, \omega, \xi^2) = \theta \cdot I(|\tilde{\theta}| > \omega)$ ,  $T_h(\theta, \omega) = \theta \cdot I(|\theta| > \omega)$  and  $T_s(\theta, \omega) = \text{sgn}(\theta)(|\theta| - \omega) \cdot I(|\theta| > \omega)$  where  $\theta \sim \mathcal{P}_\theta(\theta)$ . Then for any  $\epsilon > 0$ , there exist  $\xi^2$ , such that  $\Pr(|T_r(\theta, \omega, \xi^2) - T_h(\theta, \omega)| < \epsilon) > 0$ ,  $\Pr(|T_r(\theta, \omega, \xi^2) - \theta| < \epsilon) > 0$ , and  $\Pr(|T_r(\theta, \omega, \xi^2) - T_s(\theta^*, \omega)| < \epsilon) > 0$ , where  $\theta^* = \theta + \omega$*

when  $\theta > 0$  and  $\theta^* = \theta - \omega$  when  $\theta < 0$ . Furthermore,  $\lim_{\xi^2 \rightarrow 0} T_r(\theta, \omega, \xi^2) = T_h(\theta, \omega)$  and  $\lim_{\xi^2 \rightarrow \infty} T_r(\theta, \omega, \xi^2) = \theta$ .

Proposition 1 provides a mathematical illustration of Figure 3, which shows that relaxed-thresholded function has certain probability to reduce to soft or hard thresholded function and the flexibility is controlled by the relaxing parameter  $\xi^2$ . The proof is included in the supplementary materials.

Given a stationary kernel  $\kappa$ , we assign  $\beta_k(t) \sim \text{RTGP}(\kappa, \omega_1, \xi^2)$  for channel  $k$ . That is,

$$\beta_k(t) = E_k(t)I(|\tilde{E}_k(t)| > \omega_1), \quad E_k(t) \sim \text{GP}(0, \kappa), \quad \tilde{E}_k(t) \sim \text{N}(E_k(t), \xi^2), \quad (2)$$

where  $\{E_k(\cdot)\}_{k=1}^K$  follow independent Gaussian processes. There are various choices for the kernel function  $\kappa(\cdot, \cdot)$ ; for instance, we use the modified squared exponential (MSE) kernel, defined as:  $\kappa(x, x') = \exp\{-\alpha(|x|_2^2 + |x'|_2^2) - \rho|x - x'|_2^2\}$ , where  $\alpha > 0, \rho > 0$ , and  $|\cdot|_2$  is the  $L_2$ -norm (Wu et al. 2024, 2025). Here,  $\alpha$  is the decay parameter that controls the decay rate of variance. The parameter  $\rho$  is the smoothing parameter; a smaller value of  $\rho$  corresponds to a smoother GP. Note that the MSE kernel becomes a standard squared exponential kernel when  $\alpha = 0$ . In our study, we set the hyperparameter  $\alpha$  to a small value (0.01) and estimate  $\rho$  following the discussion in Lin et al. (2023). Specifically,  $\rho$  is estimated by averaging the estimated smoothing parameters of fitting GP models to the EEG signal on all the channels. We also include the sensitivity analysis of the hyperparameter  $\rho$  in the supplementary materials.

Similarly, for the effect of signal interaction across channels, we assign  $\zeta(k_1, k_2) \sim \text{RTGP}(\sigma_\eta^2 \kappa_I, \omega_2, \xi^2), k_1 < k_2$ , where  $\kappa_I$  represents the identity kernel. That is,

$$\begin{aligned} \zeta(k_1, k_2) &= \eta(k_1, k_2)I(|\tilde{\eta}(k_1, k_2)| > \omega_2), \\ \eta(k_1, k_2) &\stackrel{\text{iid}}{\sim} \text{N}(0, \sigma_\eta^2), \quad \tilde{\eta}(k_1, k_2) \sim \text{N}(\eta(k_1, k_2), \xi^2), \end{aligned} \quad (3)$$

and  $\sigma_\eta^2 \sim \text{IG}(a_\eta, b_\eta)$ . We choose to use the identity kernel here to assume prior independence

across channel pairs. Other kernels can be adopted when prior information is available in different applications.

By combining Model (1) with the prior specifications in (2) and (3), we define the proposed model as a Bayesian time-varying classification model with signal interactions via relaxed-thresholded Gaussian process prior (SI-RTGP).

### 3 Posterior Computation

In this section, we describe the posterior computation for Model (1) with priors (2) and (3) using probit link function. We represent the Gaussian processes by the Karhunen-Loève expansion and obtain an equivalent model representation. Specifically, consider the spectral decomposition of the kernel function,  $\kappa(x, x') = \sum_{l=1}^{\infty} \lambda_l \psi_l(x) \psi_l(x')$ , where  $\{\lambda_l\}_{l=1}^{\infty}$  are the eigenvalues in descending order, and  $\{\psi_l(x)\}_{l=1}^{\infty}$  are the corresponding orthonormal eigenfunctions. By Mercer's Theorem, we can represent the Gaussian process  $E_k(t)$  in (2) by  $E_k(t) = \sum_{l=1}^{\infty} e_{kl} \psi_l(t)$ , where  $e_{kl}$  are Karhunen-Loève coefficients. We truncate the expansion to the leading  $L$  terms, where  $L$  is chosen following the common practice in principal component analysis where we retain enough components to explain a high proportion of total variation. Then, the prior of  $\beta_k(\cdot)$  specified in (2) becomes

$$\beta_k(t) = \left\{ \sum_{l=1}^L e_{kl} \psi_l(t) \right\} I(|\tilde{E}_k(t)| > \omega_1), \quad \tilde{E}_k(t) \sim N\left(\sum_{l=1}^L e_{kl} \psi_l(t), \xi^2\right), \quad (4)$$

and  $e_{kl} \sim N(0, \sigma_e^2 \lambda_l)$ . We set  $\sigma_e^2$  to be large values and  $a_\eta = b_\eta = 0.001$  so that the priors are non-informative. For flexibility, we set  $\xi^2 = 1$  in the first 200 iterations and then gradually decrease its value to 0.0001. For  $\omega_1$  and  $\omega_2$ , we set them to zero in the first 200 steps, then assign an adaptive discrete prior, i.e.  $P(\omega_1 = \gamma_{1z}) = 1/Z$  and  $P(\omega_2 = \gamma_{2z}) = 1/Z$ ,  $z = 1, \dots, Z$ , where  $\{\gamma_{1z}\}_{z=1}^Z$  and  $\{\gamma_{2z}\}_{z=1}^Z$  are  $Z$  evenly spaced number between  $a_\omega$  quantile and  $b_\omega$  quantile of  $\{|\tilde{E}_k(t)|\}_{k=1, t=1}^{K, T}$  and  $\{|\tilde{\eta}(k_1, k_2)|\}_{k_1 < k_2}$  respectively. In practice, we found

$a_\omega = 0.25$  and  $b_\omega = 0.90$  yield good performance. We include the sensitivity analysis of  $a_\omega$  and  $b_\omega$  in the Supplementary Materials.

Given the above specifications, the full conditionals of  $\{e_{k,l}\}_{k=1,l=1}^{K,L}$ ,  $\{\tilde{E}_k(t)\}_{t=1,k=1}^{T,K}$ ,  $\{\eta(k_1, k_2)\}_{k_1 < k_2}$  and  $\{\tilde{\eta}(k_1, k_2)\}_{k_1 < k_2}$  are normal distributions due to conjugacy. The full conditionals of  $\omega_1$  and  $\omega_2$  are discrete distribution. We develop a Gibbs sampler for the posterior sampling. The detailed derivation and the sampling procedure is provided in the supplementary materials.

## 4 P300 BCI Speller Data Analysis

We analyze a publicly available P300 BCI dataset consisting of 55 participants (Won et al. 2022). EEG signals were recorded from 32 Ag/AgCl active electrodes placed according to the international 10-20 system. The signals were sampled at 512 Hz. EEG preprocessing included a bandpass filter with a frequency range of 0.5-10 Hz. Although the dataset provides a 1200 ms post-stimulus window, we restrict our analysis to the first 600 ms after stimulus onset, corresponding to 307 samples at the 512 Hz sampling rate. In the P300 speller task, participants spelled predefined words using the standard  $6 \times 6$  P300 speller paradigm, with 12 stimuli per sequence. The experiment was consisted of two phases: training (two runs) and testing (four runs). In the two training runs, participants spelled the words “BRAIN” and “POWER”. In the testing runs, they spelled four additional words, “SUBJECT,” “NEURONS,” “IMAGINE,” and “QUALITY”. During each sequence, rows and columns of the matrix flashed in a random order. Each stimulus was displayed for 125 ms, followed by a 62.5 ms pause. Each target character was flashed for 15 sequences in both training and test runs.

## 4.1 Benchmark methods and implementation details

We compare four model variants based on the proposed method, RTGP-L, RTGP-P, SIRTGP-L, and SIRTGP-P, with several commonly used classification methods. The four variants are Bayesian time-varying regression approaches that incorporate relaxed-thresholded Gaussian Process priors, using either logit (-L) or probit (-P) link functions. RTGP models include only main effects from individual EEG channels, while SIRTGP models additionally incorporate pairwise signal interactions across channels.

For benchmarking, we include GLASS (Zhao et al. 2025), EEGNet (Lawhern et al. 2018), extreme gradient boosting (XGBoost) (Sarraf, Pattnaik et al. 2023), logistic regression (Sakamoto & Aono 2009), support vector classification (SVC) (Kaper et al. 2004), random forest (RF), and stepwise linear discriminant analysis (SWLDA) (Farwell & Donchin 1988). The GLASS model is trained using the recommended default settings from the authors’ GLASS implementation (Zhao et al. 2025). Logistic regression is implemented using the scikit-learn LogisticRegression class with a maximum of 3000 iterations. SVC is implemented with the SVC class with probability estimation enabled and also uses a maximum of 3000 iterations. The random forest model uses 1000 trees, with a maximum tree depth of 3. At each split, the number of features considered is set to the square root of the total number of input features. The XGBoost model is configured with 1000 boosting rounds, a learning rate of 0.02, a maximum tree depth of 5, a column subsampling ratio of 0.8, and a regularization parameter  $\gamma = 10$ , using the binary logistic loss function. EEGNet is trained for 100 epochs with a batch size of 32, a dropout rate of 0.5, and a kernel length of 128. SWLDA is implemented using forward-backward selection with entry and removal  $p$ -value thresholds set to 0.05 and 0.1, respectively.

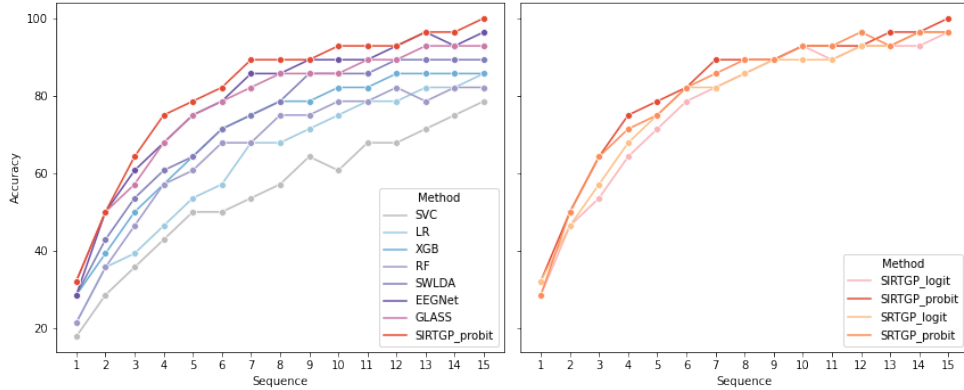


Figure 4: Median character prediction accuracy across 55 participants for different methods over 15 sequences using the proposed models (four variants) and competing methods. For clarity, the left panel includes the proposed method with channel interaction and probit link (SITRGP\_probit) and competing methods, while the right panel compares the four model variants. Competing methods include GLASS, Logistic Regression (LR), Support Vector Classifier (SVC), Random Forest (RF), Extreme Gradient Boosting (XGBoost), EEGNet, and Stepwise Linear Discriminant Analysis (SWLDA).

## 4.2 Evaluation of prediction performance

The stimulus-specific prediction output by each method, such as predicted probabilities or discrimination scores, is treated as a classification score that quantifies how likely each stimulus group (one row or one column) contains the target character. To evaluate character-level prediction accuracy, we aggregate these classification scores across sequences. Specifically, for each character, we sum the scores for all row and column stimuli across sequences and identify the predicted character as the one located at the intersection of the row and column with the highest cumulative score. To provide a more comprehensive assessment of model performance, we repeat this evaluation using the first 1 through 15 sequences. This allows us to examine how prediction accuracy improves as more sequences (i.e., repetitions of the flashing paradigm) become available.

Figure 4 presents the median character prediction accuracy across 55 participants for different methods over 15 sequences. Among the competing approaches, EEGNet and GLASS achieve the highest accuracies. However, SIRTGP-P has the highest median accuracy at every sequence comparing to competing methods. The four model variants based

Table 1: Character prediction accuracy for all methods at the last (15th) sequence. **Mean**: mean accuracy; **SD**: standard deviation; **Median**: median accuracy; **Q1**: 1st quartile for accuracy; **Q3**: 3rd quartile for accuracy.

| Method          | Mean (SD)              | Median (Q1, Q3)                  |
|-----------------|------------------------|----------------------------------|
| <b>EEGNet</b>   | 90.58% (13.65%)        | 96.43% (89.29%, 100.00%)         |
| <b>GLASS</b>    | 90.00% (14.11%)        | 92.86% (89.29%, 100.00%)         |
| <b>LR</b>       | 80.52% (20.51%)        | 85.71% (71.43%, 96.43%)          |
| <b>RF</b>       | 78.83% (19.73%)        | 82.14% (66.07%, 94.64%)          |
| <b>SVC</b>      | 70.26% (26.56%)        | 78.57% (57.14%, 91.07%)          |
| <b>SWLDA</b>    | 87.21% (15.53%)        | 89.29% (82.14%, 96.43%)          |
| <b>XGB</b>      | 84.09% (15.23%)        | 85.71% (75.00%, 96.43%)          |
| <b>RTGP-L</b>   | 90.78% (12.87%)        | 96.43% (85.71%, 100.00%)         |
| <b>RTGP-P</b>   | 92.27% (11.72%)        | 96.43% (91.07%, 100.00%)         |
| <b>SIRTGP-L</b> | 91.23% (13.67%)        | 96.43% (91.07%, 100.00%)         |
| <b>SIRTGP-P</b> | <b>92.86% (12.69%)</b> | <b>100.00% (89.29%, 100.00%)</b> |

on the proposed method have comparable performance, with the variants using the probit link slightly outperforming those using the logit link. In addition, the model variants using signal interactions achieve equal or higher median accuracy than those not using interactions at most sequences. Table 1 summarizes mean, standard deviation, median, 1st and 3rd quartiles of the character prediction accuracy using all the 15 sequences for all methods. Overall, SIRTGP-P achieves the best prediction performance, with the highest mean and median accuracy and with relatively small variations across participants. All four model variants of the proposed method outperform competing methods, with equal or higher mean and median prediction accuracy and comparatively small performance variation.

Although character-level accuracy is a fundamental performance metric for BCI systems, it does not fully reflect the user experience. In practice, users care not only about achieving high accuracy but also about how quickly that an accurate selection can be made (Ma et al. 2023). To complement the accuracy results in Figure 4, we additionally evaluate system throughput using the BCI-Utility metric. BCI-Utility is a user-centric measure that quantifies the average information gained per unit time and is maximized when a system provides both high accuracy and rapid decision-making (Dal Seno et al. 2009, Ma

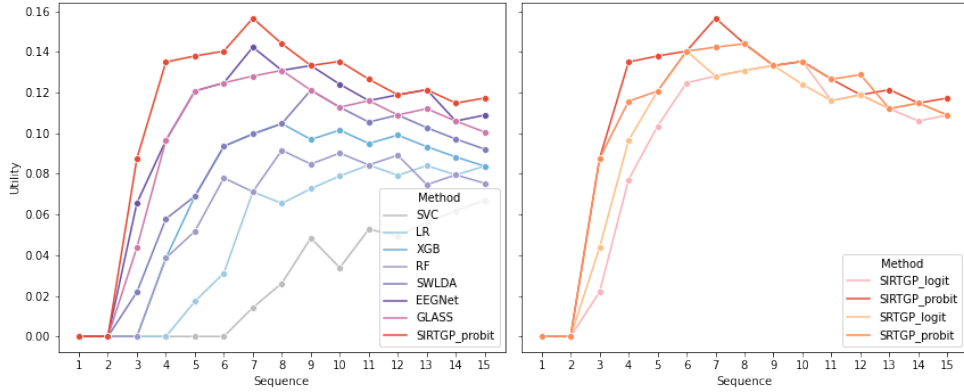


Figure 5: Median BCI-Utility (bit/second) across 55 participants for different methods over 15 sequences using the proposed models (four variants) and competing methods. For clarity, the left panel includes the proposed method with channel interaction and probit link (SITRGP\_probit) and competing methods, while the right panel compares the four model variants. Competing methods include GLASS, Logistic Regression (LR), Support Vector Classifier (SVC), Random Forest (RF), Extreme Gradient Boosting (XGBoost), EEGNet, and Stepwise Linear Discriminant Analysis (SWLDA).

et al. 2023). We compute the BCI-Utility (bit/second) for all methods using available signal up to each of the 15 sequences.

Figure 5 shows the median BCI-Utility across 55 participants. Consistent with the accuracy results, the proposed SIRTGP-P with signal interaction achieves the highest median BCI-Utility at every sequence and provides the best overall throughput among all competing methods and model variants. Importantly, BCI-Utility and accuracy do not increase monotonically over sequence in the same way. While accuracy continues to improve as more sequences of data becomes available, BCI-Utility typically peaks earlier because additional sequences increase decision time. For SIRTGP-P, the median BCI-Utility reaches its maximum at the 7th sequence, when the model already attains a high median accuracy of 89.29%, and gradually decreases thereafter, even though median accuracy continues to rise and reaches 100% at the 15th sequence. This illustrates an important trade-off. The optimal operating point for a BCI system is not necessarily the point with the highest accuracy, but the point that delivers the best balance between speed and accuracy (Ma et al. 2023). The proposed method performs strongly on both metrics, achieving the highest

accuracy while also maximizing user-centric BCI-Utility.

### 4.3 Predictive Utility and Heterogeneity of Channel Interactions

#### 4.3.1 When do channel interactions improve prediction performance?

We investigate which group of participants are more likely to benefit from incorporating the signal interaction (SI) into the prediction model. Using questionnaire data collected in the same study by Won et al. (2022), we compare the median accuracy achieved by SIRTGP-P and RTGP-P, stratified by participants' responses. Participants with prior exposure to BCI or similar biofeedback experiments show a 4% improvement in character-level accuracy when SI is included, compared to models without SI. Similarly, participants who reported abstaining from alcohol 24 hours prior to the experiment achieved a 7% gain with SI, with an maximum of 18% improvement. Additional factors associated with an increased benefit from modeling SI include feeling relaxed (+4%), being in good physical condition (+4%), finding it easy to concentrate (+2%) and perceiving the BCI task as difficult after the calibration phase (+4%). In addition, participants who reported good eye condition, high concentration, or that BCI stimuli were presented quickly during testing runs showed gains of 2-7% in accuracy when SI is included.

These findings align with the existing neuroscience literature, which has reported increased brain connectivity or regional interactions when performing familiar tasks (Terstege et al. 2022, Noad et al. 2024), being in good mental and physical state (Douw et al. 2014, Ismaylova et al. 2018, Costumero et al. 2020), making cognitive effort during tasks (Aben et al. 2020, Wang et al. 2024), and the disruptive effects of alcohol consumption on brain connectivity (Shokri-Kojori et al. 2017, Elton et al. 2021). Our results suggest that the benefit of incorporating SI in prediction models may vary between participants. Future adaptive BCI experiments could consider tailoring the use of SI predictors based on previ-

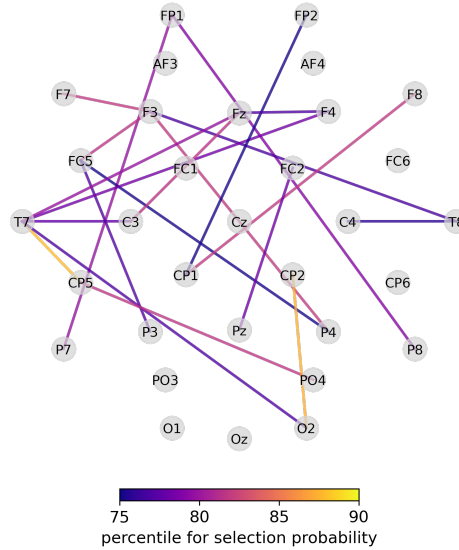


Figure 6: Average percentiles for channel interaction selection probability over the 55 participants. For clarity, only edges with percentiles greater than 75% are shown.

ous participant experience, alcohol consumption, and reported physical and mental states.

### 4.3.2 Heterogeneity in channel interaction effects

Based on the estimated SIRTGP-P signal interaction selection between-channels, we examine which pair of channels consistently contributed to the prediction performance in the 55 participants. Because a separate model is fitted for each individual, the posterior selection probability of channel interaction may not be directly comparable across individuals, we compute the percentile of the posterior channel interaction selection probability for each individual and then average these percentiles across participants for each channel pair. Figure 6 displays the channel pairs whose average percentile exceeded 75%.

We observe that the interaction between T7 and CP5 has one of the highest percentiles of selection probability, as well as the interaction between CP2 and O2. These patterns are consistent with existing neuroscience findings and are particularly relevant for the P300 BCI speller paradigm, which requires both visual-language processing and sustained attention. Both T7 and CP5 record activity from the left temporal region (Kurihara et al. 2022), and enhanced coupling within this region aligns with previous evidence of left temporal

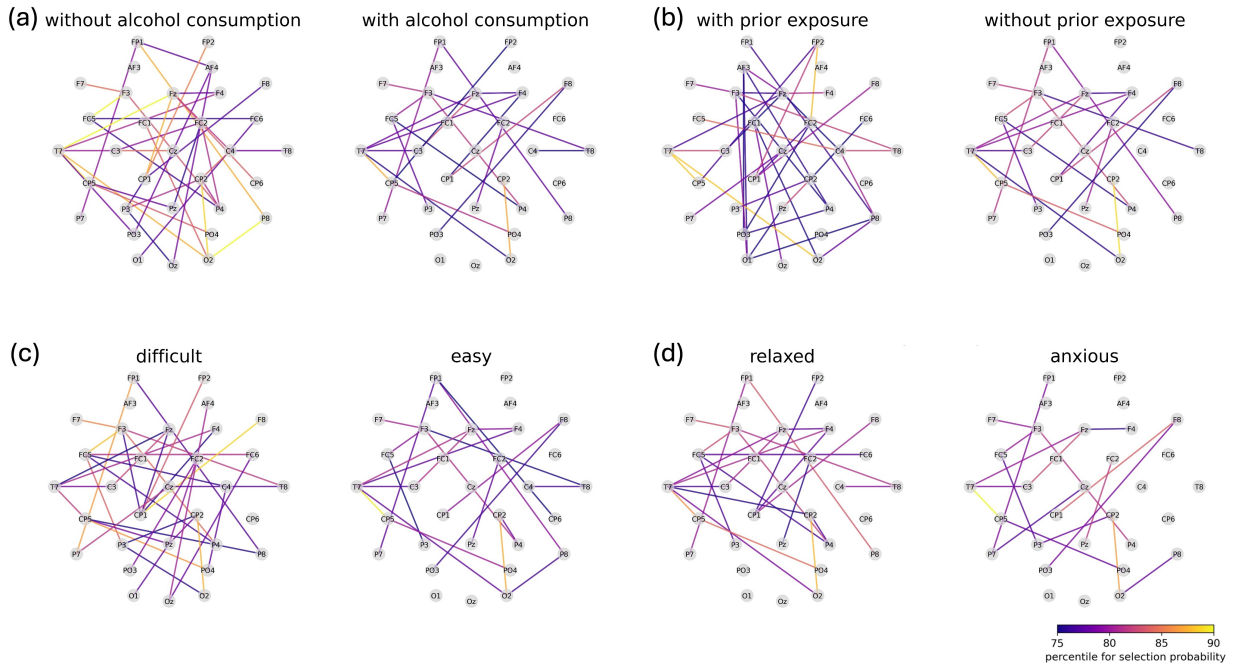


Figure 7: Average percentiles for channel interaction selection probability stratified by responses to four questions: (a) without/with alcohol consumption in 24 hours, (b) with/without prior exposure to similar experiments, (c) reported the BCI difficult/easy after experiment, and (d) reported relaxed/anxious after calibration. For clarity, only edges with percentiles greater than 75% are shown.

involvement during language-related processing (Michael et al. 2001, Trimmel et al. 2018). The CP2-O2 pair reflects parietal-occipital connectivity, and the strong effect observed here is supported by established evidence of parietal-occipital coupling during stimulus-driven visuospatial attention and during tasks involving visual and language-related processing (Indovina & Macaluso 2004, Aguilar & Grullon 2025).

To examine how channel interaction effects vary between participant groups, we plotted the average percentiles of probability of interaction selection stratified by questionnaire responses in Figure 7. The plotted network represents the subset of connectivity effects that are consistently identified as predictive. A denser network indicates that predictive information is distributed across a broader set of channel interactions, suggesting a widespread and active network-level engagement during the task. Conversely, a sparser network would imply that only a small number of specific channel-pair interactions are reliably informa-

tive. Participants who abstained from alcohol 24 hours prior to the experiment, had prior experience with similar tasks, reported the BCI typing task as difficult, or felt relaxed during the experiment exhibit denser networks on average than their respective counterparts. This suggests that channel interactions are more predictive and informative in these groups, consistent with prior evidence linking increased brain connectivity to task familiarity, mental and physical state, cognitive effort, and the absence of alcohol-related disruptions (Aben et al. 2020, Elton et al. 2021, Noad et al. 2024, Wang et al. 2024).

The T7-CP5 pair identified in Figure 6 appears in all stratified plots, while the CP2-O2 pair is observed in all stratified plots except for participants with prior exposure. Nevertheless, the relative strength of T7-CP5 and CP2-O2 vary considerably across groups, despite their presence in most plots. In general, the stratified plots exhibit substantially different patterns compared to the aggregate plot. This heterogeneity of signal interactions across participant groups highlights the value of the proposed method and helps explain why models that account for signal interactions can outperform those that do not.

#### 4.4 Temporal dynamics of channel selection

To illustrate how the proposed method identifies informative channels over time, we present the channel selection results for one representative subject. Figure 8 shows the posterior channel selection probabilities at multiple time points following stimulus onset. Panel (a) displays results from SIRTGP-P with signal interaction (SI), while panel (b) shows the corresponding results from RTGP-P without SI. The subject reported being relaxed and perceived the task as difficult. For this subject, SIRTGP-P achieves 100% prediction accuracy, which represents a 7.1% improvement (from 92.9% to 100%) over RTGP-P. This observation is consistent with our findings that participants who reported being relaxed during calibration and who found the BCI experiment difficult tend to benefit more from incorporating SI into the prediction model.

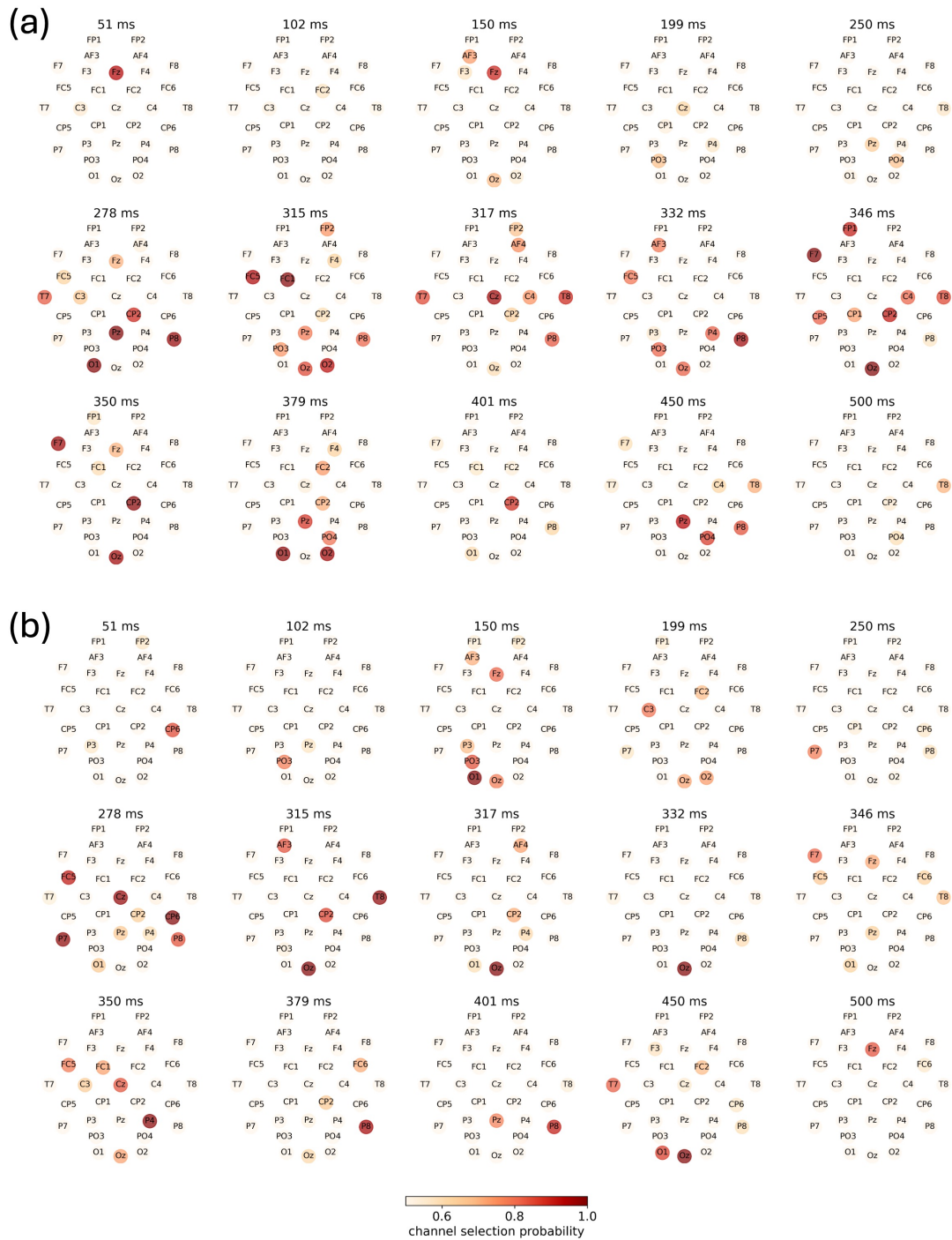


Figure 8: Posterior channel selection probability at different time points after the onset of stimulus presentation for one subject based on (a) SIRTGP-P and (b) RTGP-P.

Figure 9 presents the average target and nontarget signals across for 32 channels for the same subject. The target responses exhibit a clear and typical P300 morphology at approximately 300 ms post-stimulus (spanning 200-400 ms), which serves as the primary

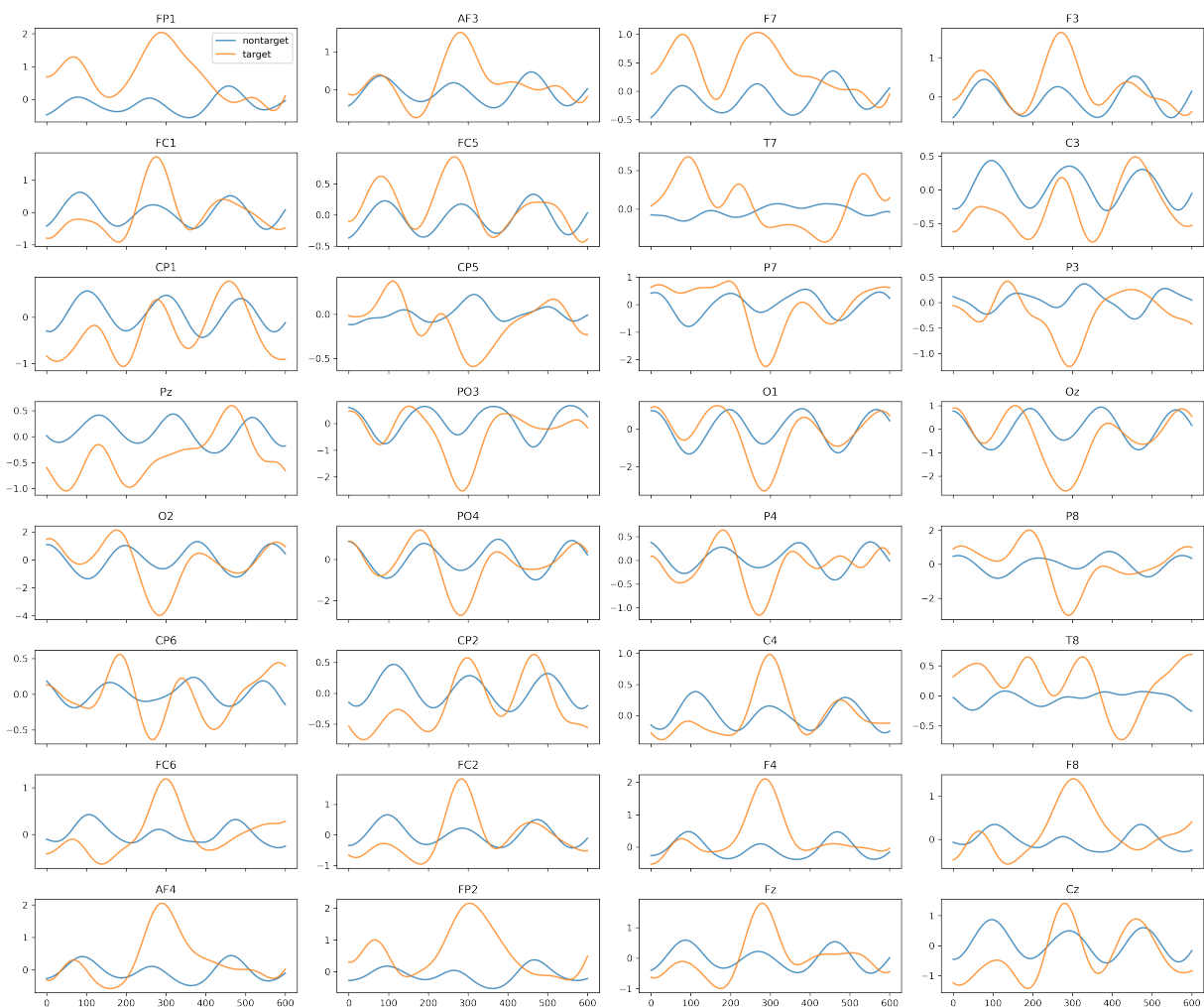


Figure 9: Average target (orange) and nontarget (blue) signals for all 32 channels from the same subject of Figure 8.

discriminative feature between target and nontarget flashes. A notable pattern emerges when comparing the two panels in Figure 8. The SI-enabled model in panel (a) identifies a larger set of informative channels around the P300 latency window. In contrast, panel (b) shows broadly similar, but consistently weaker selection patterns when SI is omitted around 300 ms. These results provide a concrete example in which explicitly modeling signal interaction enables the method to detect more spatially distributed task-relevant features and to select channels that are temporally consistent, which in turn, improves predictive performance.

## 5 Simulations

### 5.1 Data generation

We consider simulating data under a standard P300 speller setting with  $R = 19$  characters, corresponding to “THE\_QUICK\_BROWN\_FOX”, including three spaces. For each character,  $S = 5$  sequences are generated, each consisting of  $J = 12$  stimulus flashes with corresponding target and nontarget labels. To resemble realistic EEG recordings, we decompose the observed signal into stimulus-evoked components and background noise. Specifically, for channel  $k = 1, \dots, K$  and flash  $i = 1, \dots, n$ , the signal is generated as  $X_{ki}(t) = \alpha_{1k}(t)Y_i + \alpha_{0k}(t)(1 - Y_i) + \varepsilon_{1ki}(t)Y_i + \varepsilon_{0ki}(t)(1 - Y_i) + \varepsilon_{ki}(t)$ , where  $Y_i$  indicates whether the  $i$ th stimulus is a target ( $Y_i = 1$ ) or a nontarget ( $Y_i = 0$ ),  $K = 6$  is the number of channels, and  $n = R \times S \times J$ . The functions  $\alpha_{1k}(t)$  and  $\alpha_{0k}(t)$  represent the average evoked responses to target and nontarget stimuli at channel  $k$ , respectively, and are shown in Figure 10.  $\varepsilon_{1ki}(t)$  and  $\varepsilon_{0ki}(t)$  represent the noise added to the target and the nontarget stimulus respectively. The random noise  $\varepsilon_{ki}(t)$  characterizes the intrinsic brain activity of channel  $k$  unrelated to the stimulus responses. We generate the noise term as follows, for  $i = 1, \dots, n$  and  $t = 1, \dots, T$ ,  $(\varepsilon_{11i}(t), \dots, \varepsilon_{1Ki}(t))^\top \sim N(0, \tau^2 \Sigma_1)$  and  $(\varepsilon_{01i}(t), \dots, \varepsilon_{0Ki}(t))^\top \sim N(0, \tau^2 \Sigma_0)$  and  $\varepsilon_{ki}(t) \sim N(0, \sigma^2)$ , where

$$\Sigma_1 = \begin{bmatrix} 1 & \mathbf{0.7} & 0.1 & \mathbf{0.1} & 0.1 & \mathbf{0.2} \\ 0.7 & 1 & 0.1 & 0.1 & \mathbf{0.6} & 0.1 \\ 0.1 & 0.1 & 1 & \mathbf{0.7} & 0.1 & 0.1 \\ 0.1 & 0.1 & 0.7 & 1 & 0.1 & 0.1 \\ 0.1 & 0.6 & 0.1 & 0.1 & 1 & \mathbf{0.4} \\ 0.2 & 0.1 & 0.1 & 0.1 & 0.4 & 1 \end{bmatrix} \quad \text{and} \quad \Sigma_0 = \begin{bmatrix} 1 & \mathbf{0.1} & 0.1 & \mathbf{0.5} & 0.1 & \mathbf{0.8} \\ 0.1 & 1 & 0.1 & 0.1 & \mathbf{0.3} & 0.1 \\ 0.1 & 0.1 & 1 & \mathbf{0.1} & 0.1 & 0.1 \\ 0.5 & 0.1 & 0.1 & 1 & 0.1 & 0.1 \\ 0.1 & 0.3 & 0.1 & 0.1 & 1 & \mathbf{0.3} \\ 0.8 & 0.1 & 0.1 & 0.1 & 0.3 & 1 \end{bmatrix}.$$

The covariance structures  $\Sigma_1$  and  $\Sigma_0$  are designed to reflect channel-level spatial dependence under target and nontarget conditions. We generated data under varying signal and noise

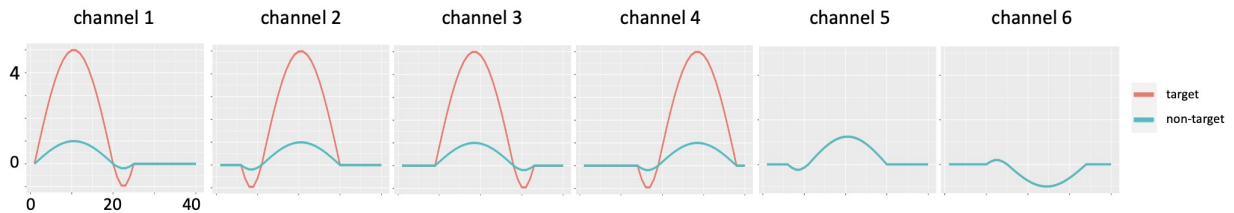


Figure 10: Channel-wise average evoked responses used in the simulation. The target and nontarget responses correspond to  $\alpha_{1k}(t)$  and  $\alpha_{0k}(t)$ , respectively.

conditions by changing the peak ratio  $\alpha$ , interaction strength  $\tau^2$ , and noise variance  $\sigma^2$ . We consider  $\alpha \in \{2.5, 3.0, 3.5\}$ ,  $\tau^2 \in \{1, 4, 9\}$ , and  $\sigma^2 \in \{20, 25, 40\}$ , where  $\alpha = 2.5$ ,  $\tau^2 = 9$ , and  $\sigma^2 = 20$  serve as the baseline configuration. We repeat each setting for 50 simulation replicates.

## 5.2 Competing methods and evaluation metrics

We consider the four variants within the RTGP framework and compare our methods with EEGNet (Lawhern et al. 2018), extreme gradient boosting (XGBoost) (Sarraf, Pattnaik et al. 2023), logistic regression (Sakamoto & Aono 2009), support vector classification (SVC) (Kaper et al. 2004), random forest (RF), and stepwise linear discriminant analysis (SWLDA) (Farwell & Donchin 1988). In addition, we include the soft-thresholded Gaussian process prior with a probit link (STGP-P) as a baseline Bayesian functional regression model, in contrast to the relaxed-thresholding mechanism adopted by the RTGP variants. All competing methods are implemented using the same software and hyperparameter settings as in Section 4.

We summarize the mean and standard deviation of character-level prediction accuracy of each method over the 50 replicates to evaluation the predictive performance. In addition, we compare the selection accuracy between the SWLDA benchmark and the proposed SI-RTGP. For channel  $k = 1, \dots, K$  and time point  $t = 1, \dots, T$ , let  $\nu_k(t) = I(|\alpha_{1k}(t) -$

$\alpha_{0k}(t) > 0$ ) denote the true signal support, and define its estimated counterpart as  $\hat{\nu}_k(t) = 1$  if  $|\hat{\beta}_k(t)| > 0$ ,  $\hat{\nu}_k(t) = 0$ , otherwise. We quantify selection performance using the effective selection window ratio (ESWR) and the exclusive effective window ratio (EEWR), defined respectively as

$$\text{ESWR}(\nu_k) = \frac{|\{t : \hat{\nu}_k(t) = 1 \ \& \ \nu_k(t) = 1\}|}{|\{t : \nu_k(t) = 1\}|}, \quad \text{EEWR}(\nu_k) = \frac{|\{t : \hat{\nu}_k(t) = 0 \ \& \ \nu_k(t) = 0\}|}{|\{t : \nu_k(t) = 0\}|}.$$

Accordingly, ESWR reflects how effectively a method recovers true signal time points, whereas EEWR reflects how effectively it excludes non-signal time points.

### 5.3 Simulation results

Table 2 reports the character-level prediction accuracy under different simulation settings. Overall, the proposed SIRTGP methods achieve the best prediction performance across all settings. In most configurations, SIRTGP-P method achieves the highest accuracy among the competing approaches.

As the peak ratio  $\alpha$  increases, prediction accuracy generally improves. The advantage of SIRTGP is most pronounced under weak main effects ( $\alpha = 2.5$ ). Under stronger main effects, several machine learning methods exhibit less stable behavior, whereas SIRTGP remains consistently competitive. Prediction accuracy decreases as the noise variance  $\sigma^2$  increases for all methods. Nevertheless, SIRTGP maintains superior performance across all noise levels. In addition, increasing  $\tau^2$  strengthens channel-level spatial dependence in the noise process. In this setting, SIRTGP achieves the largest performance gains and the best overall accuracy, which highlights the benefit of explicitly modeling interaction structure when such dependence is present.

Table 3 reports the selection accuracy results. Compared with SWLDA, SIRTGP attains substantially higher ESWR on channels with true signal activity, indicating more accurate recovery of contiguous signal-support regions. In contrast, SWLDA tends to

Table 2: Character-level prediction accuracy under different simulation settings. **Mean**: mean accuracy; **SD**: standard deviation.

(a) Different peak ratios under  $\sigma^2 = 20$  and  $\tau^2 = 9$ .

| Method   | $\alpha = 2.5$       | $\alpha = 3.0$       | $\alpha = 3.5$       |
|----------|----------------------|----------------------|----------------------|
|          | Mean (SD)            | Mean (SD)            | Mean (SD)            |
| EEGNet   | 0.804 (0.196)        | 0.916 (0.135)        | 0.784 (0.236)        |
| LR       | 0.524 (0.204)        | 0.769 (0.190)        | 0.583 (0.298)        |
| RF       | 0.502 (0.223)        | 0.769 (0.210)        | 0.545 (0.321)        |
| SVC      | 0.694 (0.220)        | 0.886 (0.147)        | 0.693 (0.278)        |
| SWLDA    | 0.689 (0.229)        | 0.885 (0.159)        | 0.683 (0.286)        |
| XGBoost  | 0.498 (0.244)        | 0.645 (0.222)        | 0.428 (0.279)        |
| STGP-P   | 0.530 (0.254)        | 0.650 (0.282)        | 0.719 (0.283)        |
| RTGP-L   | 0.715 (0.214)        | 0.882 (0.153)        | 0.952 (0.087)        |
| RTGP-P   | 0.752 (0.216)        | 0.885 (0.151)        | 0.950 (0.093)        |
| SIRTGP-L | 0.897 (0.138)        | 0.946 (0.092)        | 0.974 (0.057)        |
| SIRTGP-P | <b>0.931 (0.115)</b> | <b>0.959 (0.078)</b> | <b>0.978 (0.048)</b> |

(b) Different noise variances under  $\alpha = 2.5$  and  $\tau^2 = 9$ .

| Method   | $\sigma^2 = 20$      | $\sigma^2 = 25$      | $\sigma^2 = 40$      |
|----------|----------------------|----------------------|----------------------|
|          | Mean (SD)            | Mean (SD)            | Mean (SD)            |
| EEGNet   | 0.804 (0.196)        | 0.742 (0.213)        | 0.694 (0.237)        |
| LR       | 0.524 (0.204)        | 0.450 (0.192)        | 0.417 (0.208)        |
| RF       | 0.502 (0.223)        | 0.415 (0.201)        | 0.370 (0.228)        |
| SVC      | 0.694 (0.220)        | 0.611 (0.220)        | 0.560 (0.244)        |
| SWLDA    | 0.689 (0.229)        | 0.605 (0.230)        | 0.548 (0.252)        |
| XGBoost  | 0.498 (0.244)        | 0.408 (0.274)        | 0.393 (0.261)        |
| STGP-P   | 0.530 (0.254)        | 0.493 (0.244)        | 0.405 (0.208)        |
| RTGP-L   | 0.715 (0.214)        | 0.662 (0.218)        | 0.506 (0.200)        |
| RTGP-P   | 0.752 (0.216)        | 0.691 (0.223)        | 0.547 (0.214)        |
| SIRTGP-L | 0.897 (0.138)        | 0.860 (0.160)        | 0.700 (0.209)        |
| SIRTGP-P | <b>0.931 (0.115)</b> | <b>0.893 (0.150)</b> | <b>0.768 (0.207)</b> |

(c) Different interaction strengths under  $\alpha = 2.5$  and  $\sigma^2 = 20$ .

| Method   | $\tau^2 = 1$         | $\tau^2 = 4$         | $\tau^2 = 9$         |
|----------|----------------------|----------------------|----------------------|
|          | Mean (SD)            | Mean (SD)            | Mean (SD)            |
| EEGNet   | 0.434 (0.191)        | 0.810 (0.221)        | 0.804 (0.196)        |
| LR       | 0.829 (0.185)        | 0.603 (0.273)        | 0.524 (0.204)        |
| RF       | 0.588 (0.224)        | 0.576 (0.299)        | 0.502 (0.223)        |
| SVC      | 0.749 (0.205)        | 0.727 (0.259)        | 0.694 (0.220)        |
| SWLDA    | 0.762 (0.212)        | 0.723 (0.266)        | 0.689 (0.229)        |
| XGBoost  | 0.572 (0.237)        | 0.536 (0.238)        | 0.498 (0.244)        |
| STGP-P   | 0.618 (0.276)        | 0.582 (0.274)        | 0.530 (0.254)        |
| RTGP-L   | 0.828 (0.177)        | 0.787 (0.193)        | 0.715 (0.214)        |
| RTGP-P   | <b>0.837 (0.181)</b> | 0.801 (0.201)        | 0.752 (0.216)        |
| SIRTGP-L | 0.801 (0.186)        | 0.834 (0.170)        | 0.897 (0.138)        |
| SIRTGP-P | 0.827 (0.190)        | <b>0.863 (0.163)</b> | <b>0.931 (0.115)</b> |

Table 3: Selection accuracy measured by ESWR and EEWR under  $\alpha = 2.5$ ,  $\sigma^2 = 20$ , and  $\tau^2 = 9$ . The reported numbers are Mean (SD) across simulation replications.

|      | Method | Ch 1          | Ch 2          | Ch 3          | Ch 4          | Ch 5          | Ch 6          |
|------|--------|---------------|---------------|---------------|---------------|---------------|---------------|
| ESWR | SIRTGP | 0.465 (0.103) | 0.518 (0.144) | 0.479 (0.100) | 0.497 (0.123) | –             | –             |
|      | SWLDA  | 0.393 (0.067) | 0.395 (0.055) | 0.378 (0.066) | 0.425 (0.082) | –             | –             |
| EEWR | SIRTGP | 0.918 (0.087) | 0.940 (0.073) | 0.944 (0.090) | 0.941 (0.074) | 0.960 (0.046) | 0.971 (0.039) |
|      | SWLDA  | 0.936 (0.052) | 0.934 (0.067) | 0.949 (0.058) | 0.935 (0.059) | 0.947 (0.031) | 0.941 (0.034) |

select isolated time points, which leads to reduced coverage of the true signal window. Meanwhile, both methods achieve comparably high EEWR, suggesting effective control of false discoveries in non-signal regions.

## 6 Conclusion

In this study, we propose a Bayesian time-varying regression model with channel interactions via the relaxed-thresholded Gaussian process (RTGP) priors for P300 BCI speller. The proposed SIRTGP models achieves the overall best predictive performance under varying signal and noise conditions in simulation, and shows superior temporal channel selection compared with the baseline method. The application of SIRTGP on a publicly available dataset demonstrates its real-world advantage compared to common predictive models used in P300 speller. Furthermore, through the proposed framework, we identify key channels and channel pairs that contribute to P300 detection, which offers insights for future BCI study and neural signal modeling.

## Data and Code Availability

The data used this study is from a publicly available EEG dataset for RSVP and P300 speller brain-computer interface experiments (Won et al. 2022). The dataset is openly accessible at <https://doi.org/10.6084/m9.figshare.c.5769449>. Our method has a Python implementation and is available at <https://github.com/yuxiao-66/rtgp>.

## References

- Aben, B., Calderon, C. B., Van den Bussche, E. & Verguts, T. (2020), ‘Cognitive effort modulates connectivity between dorsal anterior cingulate cortex and task-relevant cortical areas’, *Journal of Neuroscience* **40**(19), 3838–3848.
- Aguilar, O. & Grullon, R. (2025), ‘Spatial dynamics and functional connectivity in eeg: Insights from lexical processing’, *bioRxiv* pp. 2025–04.
- Barthélemy, Q., Chevallier, S., Bertrand-Lalo, R. & Clisson, P. (2023), ‘End-to-end p300 bci using bayesian accumulation of riemannian probabilities’, *Brain-Computer Interfaces* **10**(1), 50–61.
- Cai, Q., Kang, J. & Yu, T. (2020), ‘Bayesian network marker selection via the thresholded graph laplacian gaussian prior’, *Bayesian Analysis* **15**(1), 79.
- Costumero, V., Bueichekú, E., Adrián-Ventura, J. & Ávila, C. (2020), ‘Opening or closing eyes at rest modulates the functional connectivity of v1 with default and salience networks’, *Scientific reports* **10**(1), 9137.
- Dal Seno, B., Matteucci, M. & Mainardi, L. T. (2009), ‘The utility metric: a novel method to assess the overall performance of discrete brain–computer interfaces’, *IEEE Transactions on Neural Systems and Rehabilitation Engineering* **18**(1), 20–28.
- Ditthapron, A., Banluesombatkul, N., Ketrat, S., Chuangsuwanich, E. & Wilaiprasitporn, T. (2019), ‘Universal joint feature extraction for p300 eeg classification using multi-task autoencoder’, *IEEE Access* **7**, 68415–68428.
- Douw, L., Nieboer, D., van Dijk, B. W., Stam, C. J. & Twisk, J. W. (2014), ‘A healthy brain in a healthy body: brain network correlates of physical and mental fitness’, *PLoS One* **9**(2), e88202.

- Elton, A., Garbutt, J. C. & Boettiger, C. A. (2021), ‘Risk and resilience for alcohol use disorder revealed in brain functional connectivity’, *NeuroImage: Clinical* **32**, 102801.
- Farwell, L. A. & Donchin, E. (1988), ‘Talking off the top of your head: toward a mental prosthesis utilizing event-related brain potentials’, *Electroencephalography and clinical Neurophysiology* **70**(6), 510–523.
- Fazel-Rezai, R., Allison, B. Z., Guger, C., Sellers, E. W., Kleih, S. C. & Kübler, A. (2012), ‘P300 brain computer interface: current challenges and emerging trends’, *Frontiers in neuroengineering* **5**, 14.
- Friston, K. J., Buechel, C., Fink, G. R., Morris, J., Rolls, E. & Dolan, R. J. (1997), ‘Psychophysiological and modulatory interactions in neuroimaging’, *Neuroimage* **6**(3), 218–229.
- Griffin, J. & Brown, P. (2017), ‘Hierarchical shrinkage priors for regression models’, *Bayesian Analysis* **12**(1), 135–159.
- Hao, N., Feng, Y. & Zhang, H. H. (2018), ‘Model selection for high-dimensional quadratic regression via regularization’, *Journal of the American Statistical Association* **113**(522), 615–625.
- Indovina, I. & Macaluso, E. (2004), ‘Occipital–parietal interactions during shifts of exogenous visuospatial attention: trial-dependent changes of effective connectivity’, *Magnetic resonance imaging* **22**(10), 1477–1486.
- Ismaylova, E., Di Sante, J., Gouin, J.-P., Pomares, F. B., Vitaro, F., Tremblay, R. E. & Booij, L. (2018), ‘Associations between daily mood states and brain gray matter volume, resting-state functional connectivity and task-based activity in healthy adults’, *Frontiers in Human Neuroscience* **12**, 168.

- Kabbara, A., Khalil, M., El-Falou, W., Eid, H. & Hassan, M. (2016), ‘Functional brain connectivity as a new feature for p300 speller’, *PLoS One* **11**(1), e0146282.
- Kang, J., Reich, B. J. & Staicu, A.-M. (2018), ‘Scalar-on-image regression via the soft-thresholded gaussian process’, *Biometrika* **105**(1), 165–184.
- Kaper, M., Meinicke, P., Grossekhoefer, U., Lingner, T. & Ritter, H. (2004), ‘Bci competition 2003-data set iib: support vector machines for the p300 speller paradigm’, *IEEE Transactions on biomedical Engineering* **51**(6), 1073–1076.
- Kshirsagar, G. B. & Londhe, N. D. (2019), ‘Weighted ensemble of deep convolution neural networks for single-trial character detection in devanagari-script-based p300 speller’, *IEEE Transactions on Cognitive and Developmental Systems* **12**(3), 551–560.
- Kurihara, Y., Takahashi, T. & Osu, R. (2022), ‘The relationship between stability of interpersonal coordination and inter-brain eeg synchronization during anti-phase tapping’, *Scientific reports* **12**(1), 6164.
- Kwak, N.-S., Müller, K.-R. & Lee, S.-W. (2015), ‘A lower limb exoskeleton control system based on steady state visual evoked potentials’, *Journal of neural engineering* **12**(5), 056009.
- Lawhern, V. J., Solon, A. J., Waytowich, N. R., Gordon, S. M., Hung, C. P. & Lance, B. J. (2018), ‘Eegnet: a compact convolutional neural network for eeg-based brain–computer interfaces’, *Journal of neural engineering* **15**(5), 056013.
- Lin, Z., Si, Y. & Kang, J. (2023), ‘Latent subgroup identification in image-on-scalar regression’, *arXiv preprint arXiv:2307.00129* .
- Ma, G., Kang, J., Thompson, D. E. & Huggins, J. E. (2023), ‘Bci-utility metric for asyn-

- chronous p300 brain-computer interface systems’, *IEEE Transactions on Neural Systems and Rehabilitation Engineering* **31**, 3968–3977.
- Ma, T., Li, Y., Huggins, J. E., Zhu, J. & Kang, J. (2022), ‘Bayesian inferences on neural activity in eeg-based brain-computer interface’, *Journal of the American Statistical Association* **117**(539), 1122–1133.
- Michael, E. B., Keller, T. A., Carpenter, P. A. & Just, M. A. (2001), ‘fmri investigation of sentence comprehension by eye and by ear: Modality fingerprints on cognitive processes’, *Human brain mapping* **13**(4), 239–252.
- Noad, K. N., Watson, D. M. & Andrews, T. J. (2024), ‘Familiarity enhances functional connectivity between visual and nonvisual regions of the brain during natural viewing’, *Cerebral Cortex* **34**(7), bhae285.
- Pfurtscheller, G., Müller-Putz, G. R., Scherer, R. & Neuper, C. (2008), ‘Rehabilitation with brain-computer interface systems’, *Computer* **41**(10), 58–65.
- Philip, J. T. & George, S. T. (2020), ‘Visual p300 mind-speller brain-computer interfaces: a walk through the recent developments with special focus on classification algorithms’, *Clinical EEG and neuroscience* **51**(1), 19–33.
- Sakamoto, Y. & Aono, M. (2009), Supervised adaptive downsampling for P300-based brain-computer interface, in ‘2009 Annual International Conference of the IEEE Engineering in Medicine and Biology Society’, IEEE, pp. 567–570.
- Sarraf, J., Pattnaik, P. et al. (2023), ‘A study of classification techniques on P300 speller dataset’, *Materials Today: Proceedings* **80**, 2047–2050.
- Shi, R. & Kang, J. (2015), ‘Thresholded multiscale gaussian processes with applica-

- tion to bayesian feature selection for massive neuroimaging data’, *arXiv preprint arXiv:1504.06074* .
- Shokri-Kojori, E., Tomasi, D., Wiers, C. E., Wang, G.-J. & Volkow, N. D. (2017), ‘Alcohol affects brain functional connectivity and its coupling with behavior: greater effects in male heavy drinkers’, *Molecular psychiatry* **22**(8), 1185–1195.
- Terstege, D. J., Durante, I. M. & Epp, J. R. (2022), ‘Brain-wide neuronal activation and functional connectivity are modulated by prior exposure to repetitive learning episodes’, *Frontiers in Behavioral Neuroscience* **16**, 907707.
- Tononi, G. & Edelman, G. M. (1998), ‘Consciousness and complexity’, *science* **282**(5395), 1846–1851.
- Trimmel, K., van Graan, A. L., Caciagli, L., Haag, A., Koepp, M. J., Thompson, P. J. & Duncan, J. S. (2018), ‘Left temporal lobe language network connectivity in temporal lobe epilepsy’, *Brain* **141**(8), 2406–2418.
- Van Erp, J., Lotte, F. & Tangermann, M. (2012), ‘Brain-computer interfaces: beyond medical applications’, *Computer* **45**(4), 26–34.
- Wang, C., Jiang, B. & Zhu, L. (2021), ‘Penalized interaction estimation for ultrahigh dimensional quadratic regression’, *Statistica Sinica* **31**(3), 1549–1570.
- Wang, W., Li, H., Wang, Y., Liu, L. & Qian, Q. (2024), ‘Changes in effective connectivity during the visual-motor integration tasks: a preliminary f-nirs study’, *Behavioral and Brain Functions* **20**(1), 4.
- Won, K., Kwon, M., Ahn, M. & Jun, S. C. (2022), ‘EEG dataset for RSVP and P300 speller brain-computer interfaces’, *Scientific data* **9**(1), 388.

- Wu, B., Guo, Y. & Kang, J. (2024), ‘Bayesian spatial blind source separation via the thresholded gaussian process’, *Journal of the American Statistical Association* **119**(545), 422–433.
- Wu, B., Wu, K. & Kang, J. (2025), ‘Bayesian scalar-on-image regression with a spatially varying single-layer neural network prior’, *Journal of Machine Learning Research* **26**(116), 1–38.
- Xu, N., Gao, X., Hong, B., Miao, X., Gao, S. & Yang, F. (2004), ‘Bci competition 2003-data set iib: enhancing p300 wave detection using ica-based subspace projections for bci applications’, *IEEE transactions on biomedical engineering* **51**(6), 1067–1072.
- Xu, Y., Johnson, T. D., Heitzeg, M. & Kang, J. (2026), ‘Bayesian image mediation analysis’, *Journal of the American Statistical Association* **In Press**.
- Xu, Y. & Kang, J. (2025), Bayesian image regression with soft-thresholded conditional autoregressive prior, *in* ‘The Thirteenth International Conference on Learning Representations’.
- Zhang, Y., Zhou, G., Jin, J., Zhao, Q., Wang, X. & Cichocki, A. (2015), ‘Sparse bayesian classification of eeg for brain–computer interface’, *IEEE transactions on neural networks and learning systems* **27**(11), 2256–2267.
- Zhao, B., Huggins, J. E. & Kang, J. (2025), ‘Bayesian inference on brain-computer interfaces via glass’, *Journal of the American Statistical Association* **In Press**.